

# Thin accretion disks are stabilized by a strong magnetic field

Aleksander Sądowski<sup>1,2\*</sup>

<sup>1</sup> MIT Kavli Institute for Astrophysics and Space Research 77 Massachusetts Ave, Cambridge, MA 02139, USA

<sup>2</sup> Einstein Fellow

12 May 2018

## ABSTRACT

By studying three-dimensional, radiative, global simulations of sub-Eddington, geometrically thin black hole accretion flows we show that thin disks which are dominated by magnetic pressure are stable against thermal instability. Such disks are thicker than predicted by the standard model and show significant amount of dissipation inside the marginally stable orbit. Radiation released in this region, however, does not escape to infinity but is advected into the black hole. We find that the resulting accretion efficiency ( $5.5 \pm 0.5\%$  for the simulated  $0.8\dot{M}_{\text{Edd}}$  disk) is very close to the predicted by the standard model (5.7%).

**Key words:** accretion, accretion discs – black hole physics – relativistic processes – methods: numerical

## 1 INTRODUCTION

Most of the Galactic black hole (BH) X-ray binaries cycle through outbursts and quiescent states as a result of modulation of the accretion rate by ionization instability in the outer disk regions (Lasota 2001; Coriat et al. 2012). During the outbursts they show luminosities of the order of 1 – 30% of the Eddington luminosity,  $L_{\text{Edd}}$  (Maccarone 2003; McClintock & Remillard 2006). According to the standard disk theory (Shakura & Sunyaev 1973), such luminosities correspond to the radiation-pressure dominated, radiatively efficient disk state. X-ray binaries can remain in such a configuration for months, i.e., for the time much longer than the relevant dynamical, thermal, or even viscous timescales. However, radiation-pressure dominated thin disks are known to be viscously (Lightman & Eardley 1974) and thermally (Shakura & Sunyaev 1976) unstable. If such instabilities operate, one should expect global limit cycle behavior (Lasota & Pelat 1991; Szuszkiewicz & Miller 1998)<sup>1</sup>, instead of the observed quasi-steady high/soft state of most BH X-ray binaries. The disagreement strongly suggests that our understanding of the physics of thin disk accretion is not satisfactory.

Accretion flows are known to be turbulent. Because of this fact the value of analytical modeling is limited and numerical simulations are required for better understanding them. Recently, significant progress has been made through development of sophisticated magnetohydrodynamical (MHD) and radiation MHD (RMHD) codes capable of simulating accretion flows both in the shearing box approximation and in the global context. The application of the latter has so far been limited to studying geometrically thick accretion disks (e.g., Ohsuga & Mineshige 2011; Sądowski et al. 2014b; McKinney et al. 2014; Jiang et al. 2014) which are

known (the optically thick ones) to be stabilized by advection-related cooling (Abramowicz et al. 1988). The only insight into the physics of geometrically thin, radiation-pressure dominated and presumably unstable accretion flows has come so far from shearing box simulations. Most recently, Jiang, Stone, & Davis (2013) studied such systems (with zero net magnetic flux) using a sophisticated radiation MHD algorithm and have shown that they are indeed unstable, in disagreement with most of the observed systems.

What does stabilize the astrophysical thin disks? A wide range of ideas has been proposed, including stabilization by stochastic variability (Janiuk & Misra 2012), intrinsic delay between heating and cooling (Hirose et al. 2009; Ciesielski et al. 2012), and magnetic fields. The latter seem to be most promising as magnetic fields are intrinsically involved in every accretion event (they make the disks turbulent), and probably are also crucial in explaining the observed nature of state transitions (Begelman & Armitage 2014).

Begelman & Pringle (2007) claimed that optically thick, geometrically thin accretion disks with strong toroidal magnetic field are stable against thermal and viscous instabilities. The authors based on the assumption that the field strength for a thin disk saturates at the level derived by Pessah & Psaltis (2005), i.e., when the Alfvén speed roughly equals the geometric mean of the Keplerian speed and the speed of sound in gas. We do not find this condition satisfied in the simulated thin disks presented in this work. Oda et al. (2009) discussed the stabilizing effect of strong toroidal magnetic field on thermal stability of optically thin and thick accretion disks using analytical approach and an ad hoc, although physically motivated, prescription for the radial distribution of the magnetic flux. Our work essentially validates their assumptions and conclusions. Recently, Li & Begelman (2014) have shown that magnetic fields may help stabilize the disk also through magnetically driven outflows which decrease the disk temperature and thus help the disk become more stable at a given accretion rate.

In this work we show that indeed, magnetically supported thin

\* E-mail: asadowsk@mit.edu (AS)

<sup>1</sup> Which may be responsible for some of the variability patterns of the outliers in the X-ray binary set – GRS 1915+105 and IGR J17091-3624.

disks are stable against thermal instability. We perform two three-dimensional global simulations of radiative, sub-Eddington accretion flows using a state-of-the-art general relativistic RMHD code. The simulated accretion flows led to strongly and weakly magnetized states. Only the former reached thermal equilibrium. The latter showed significant and consistent excess of cooling. Our work should be considered as a proof of principle. More numerical effort is necessary to understand the properties of the magnetically supported accretion disks across the spectrum of accretion rates and large scale properties of magnetic field.

Our work is organized as follows. In Section 2 we show with a simple argument that magnetically supported disks are thermally stable. In Section 3 we present the numerical methods we applied and the initial conditions for the simulations we performed. In Section 4 we discuss the differences in the ultimate magnetic field configuration. In Section 5 we compute and compare rates of heating and cooling. The collapse of the weakly magnetized disk is discussed in Section 6. The properties of the stable solution are presented in Sections 7 and 8, and are followed by Discussion and Summary.

In this work we adopt the following definition for the Eddington mass accretion rate,

$$\dot{M}_{\text{Edd}} = \frac{L_{\text{Edd}}}{\eta c^2}, \quad (1)$$

where  $L_{\text{Edd}} = 1.25 \times 10^{38} M/M_{\odot}$  ergs/s is the Eddington luminosity, and  $\eta$  is the radiative efficiency of a thin disk around a black hole with a given spin  $a_* \equiv a/M$ . For zero BH spin,  $\eta \approx 0.057$  and  $\dot{M}_{\text{Edd}} = 2.48 \times 10^{18} M/M_{\odot}$  g/s. Hereafter, we also use the gravitational radius  $r_g = GM/c^2$  as the unit of length, and  $t_g = r_g/c$  as the unit of time.

## 2 MAGNETIC PRESSURE MAKES THIN DISKS THERMALLY STABLE

Radiation pressure-dominated disks are known to exhibit thermal instability coming from the fact that viscous heating responds more rapidly to changes in midplane pressure than the radiative cooling (Pringle 1976; Piran 1978). The former is given through,

$$Q^+ = \alpha P_{\text{tot}} \frac{d\Omega_K}{dr} \approx \alpha p_{\text{rad}} h \frac{d\Omega}{dr} \quad (2)$$

where  $\alpha$  is the standard viscosity parameter,  $\Omega_K$  is the Keplerian angular velocity,  $h$  is disk thickness, and  $P$  and  $p$  denote vertically integrated and central pressures, respectively. Taking into account the equation of vertical equilibrium,

$$\Omega_K^2 h^2 = \frac{P_{\text{tot}}}{\Sigma} = \frac{p_{\text{rad}} h}{\Sigma}, \quad (3)$$

one gets,

$$Q^+ = \alpha p_{\text{rad}}^2 \frac{\Sigma}{\Omega_K^2} \frac{d\Omega}{dr}. \quad (4)$$

Therefore, in the case of a radiation pressure dominated disk, the viscous heating depends on the central pressure, here - radiation pressure, as,

$$\left. \frac{d \log Q^+}{d \log p_{\text{rad}} \Big|_{\Sigma}} \right|_{\Sigma} = 2. \quad (5)$$

Radiative cooling in the diffusive approximation is given through,

$$Q^- = \frac{p_{\text{rad}}}{\Sigma \kappa}, \quad (6)$$

with  $\kappa$  being the opacity coefficient (assumed constant), and depends on the central pressure as,

$$\left. \frac{d \log Q^-}{d \log p_{\text{rad}} \Big|_{\Sigma}} \right|_{\Sigma} = 1. \quad (7)$$

Weaker slope means that whenever the central pressure gets perturbed, the heating responds stronger what causes either runaway heating or cooling (for numerical example of such behavior see Jiang, Stone, & Davis 2013).

Let us now introduce the magnetization parameter  $\beta' = p_{\text{mag}}/p_{\text{tot}}$ , equal to the ratio of magnetic to total pressures, and let us neglect the gas thermal pressure. The rate of radiative cooling is insensitive to the magnetic pressure and Eqs. 6 and 7 hold. The heating rate, however, now equals,

$$Q^+ = \alpha P_{\text{tot}} \frac{d\Omega_K}{dr} = \frac{\alpha p_{\text{rad}}^2}{(1-\beta')^2} \frac{\Sigma}{\Omega_K^2} \frac{d\Omega}{dr}. \quad (8)$$

Taking into account that,

$$\left. \frac{d\beta'}{dp_{\text{rad}}} \Big|_{p_{\text{mag}}} \right|_{p_{\text{mag}}} = -\frac{\beta(1-\beta)}{p_{\text{rad}}}, \quad (9)$$

we get,

$$\left. \frac{d \log Q^+}{d \log p_{\text{rad}} \Big|_{\Sigma, p_{\text{mag}}}} \right|_{\Sigma, p_{\text{mag}}} = 2(1-\beta'), \quad (10)$$

what, in the limit of insignificant magnetic field ( $\beta' = 0$ ) recovers the standard result (Eq. 5). However, if only the magnetic field dominates the pressure budget, i.e., when  $\beta' > 1/2$ , the heating rate does no longer increase more rapidly with the central radiation pressure than the cooling rate and the disk stabilizes itself. In other words, change of the radiation pressure at the midplane (resulting, e.g., from gas changing its temperature) does no longer efficiently translate into the change of the total integrated pressure (which determines the rate of heating).

## 3 NUMERICAL METHODS

We use general relativistic (GR) radiation magnetohydrodynamical (RMHD) code KORAL (Sądowski et al. 2013a, 2014a). It evolves gas, magnetic field and radiation field in a fixed spacetime described by an arbitrary metric. Magnetic fields are evolved under the assumption of ideal MHD, i.e., we assume that the electric field vanishes in the gas comoving frame, and there is no explicit resistive term. The gas is coupled to radiation through the radiation four-force describing the energy and momentum exchange through absorption and scattering. We use the basic thermal Comptonization as described in Sądowski et al. (2014b). We evolve four quantities describing the radiation field, corresponding to the radiative energy density and momentum. The radiation stress-energy tensor is closed using the M1 closure (Levermore 1984; Sądowski et al. 2013a). In addition, we use the radiative viscosity prescription given in the Appendix of Sądowski et al. (2014b). We adopted the following formulae for the absorption and scattering opacities,  $\kappa_{\text{abs}}$  and  $\kappa_{\text{es}}$ , respectively,

$$\kappa_{\text{abs}} = 6.4 \times 10^{22} \rho T^{-7/2} \text{ cm}^2/\text{g}, \quad (11)$$

$$\kappa_{\text{es}} = 0.34 \text{ cm}^2/\text{g}. \quad (12)$$

We adopt the Kerr-Shield metric and the radial cells are distributed exponentially in radius, with the innermost five cells located inside the BH horizon. The polar cells are concentrated towards the equatorial plane to provide higher resolution in the disk region (the

effective vertical resolution for simulations presented here, calculated basing on the vertical cell size at the equatorial plane, is  $N_{\theta, \text{eff}} = 1250$ ). The azimuthal cells are distributed uniformly.

### 3.1 Initial state and simulation sequence

Simulating radiation pressure dominated, geometrically thin accretion disks requires careful choice of initial conditions. One can easily imagine that if the initial state is too far from the equilibrium solution, one may “overshoot” and instead of finding the intended solution at the middle, presumably unstable branch of the temperature-surface density diagram (the so-called S-curve, Abramowicz et al. 1988), one may find a solution at the lower, gas-pressure dominated branch corresponding to lower accretion rates, or at the upper, advection-dominated branch.

The standard way of initializing simulations of accretion disks is to start from an equilibrium torus of gas threaded by weak poloidal magnetic field. As a result of magnetorotational instability (MRI, Balbus & Hawley 1991) this magnetic field triggers turbulence and the related dissipative heating. Using the same setup for simulating thin disks may be problematic. Firstly, the initial torus may contaminate the most interesting inner region of the disk by, e.g., blocking radiation coming from that region. Secondly, if one starts from a thin, radiation pressure supported torus of low optical depth, the torus may cool significantly (on the thermal timescale,  $t_{\text{th}} \approx 1/\alpha\Omega$ ) by the time the turbulence triggers in (on the dynamical timescale,  $t_{\text{dyn}} \approx 1/\Omega$ ), especially for large viscosity  $\alpha$  parameters, typical for inner regions of accretion (Penna et al. 2013).

We decided to follow a different approach. We start from a relatively optically thick torus located far from the BH. We evolve that torus in axisymmetry to let the gas reach the innermost region and start crossing the BH horizon. Then, the gas, magnetic field and radiation are rewritten onto a three-dimensional grid. The simulation is continued in three-dimensions and gives mildly super-Eddington solution. Then, in the second step, the gas density and magnetic field are scaled down by constant factors keeping fixed the gas temperature and magnetic to gas pressure ratio. As a result, we start the ultimate simulation from a state which is already turbulent and presumably close to the equilibrium corresponding to a sub-Eddington accretion flow.

We have simulated three models, the parameters of which are specified in Table 1. Two fiducial simulations (Q and D) were initiated with the same torus but with different configurations of magnetic field (discussed below) and both were evolved in three dimensions with the azimuthal wedge limited, for the sake of computational cost, to  $\pi/2$ . The third simulation, Q( $2\pi$ ), was performed with the full  $2\pi$  wedge, ran for a limited time, and have shown very similar properties to simulation Q. For this reason, we will compare only simulations Q and D below.

### 3.2 Initial magnetic field

In Section 2 we argued that a thin, radiatively efficient accretion disk with radiation pressure dominating over gas pressure is thermally stable if magnetic pressure overcomes the radiation pressure and provides most of the pressure support. Such conditions are not satisfied in the standard saturation state of magnetorotational instability (MRI). Sophisticated simulations of shearing boxes have shown that the typical magnetic to total pressure ratio is only 10% (e.g., Davis et al. 2010; Shi et al. 2010). This number increases for simulations with non-zero net vertical magnetic flux. For suffi-

**Table 1.** Model parameters

Name	$\dot{M}_{\text{BH}}/\dot{M}_{\text{Edd}}$	$\Delta t$	$\Delta\phi$	$N_r \times N_\theta \times N_\phi$	$B_{\text{init}}$
Q	0.82	$20000r_g$	$\pi/2$	$320 \times 320 \times 32$	quad.
Q( $2\pi$ )	0.80	$5000r_g$	$2\pi$	$320 \times 320 \times 128$	quad.
D	$1 \searrow$	$9200r_g$	$\pi/2$	$320 \times 320 \times 32$	dipolar

$\dot{M}_{\text{BH}}$  - average accretion rate through the BH horizon,

$\Delta t$  - duration of the simulation,  $\Delta\phi$  - wedge in azimuth,

$N_r \times N_\theta \times N_\phi$  - resolution in radius, polar and azimuthal angles,

$B_{\text{init}}$  - configuration of the initial magnetic field.

Other parameters:  $M_{\text{BH}} = 10M_\odot$ ,  $a_* = 0$ ,  $r_{\text{in}} = 1.85$ ,  $r_{\text{out}} = 500$ ,

effective resolution in polar angle at the equatorial plane,  $N_{\theta, \text{eff}} = 1250$ .

ciently strong fluxes the entire shearing box may become magnetically dominated (Bai & Stone 2013).

Simulations of accretion flows in the shearing box approximation do not allow for radial advection of heat or magnetic field. They also neglect the curvature terms (the characteristic radius is infinity). What is more, one cannot start a simulation with a non-zero radial flux of magnetic field – the shear converts the radial component of magnetic field into azimuthal one and leads to unlimited grow of the magnetic field. Such a behavior, however, does not have to occur in a global simulation, where the growing magnetic field can be advected or escape from the disk.

In this work we aim at comparing properties of strongly and weakly magnetized thin accretion disks. Having in mind that the large scale configuration of the magnetic field has an impact on the level of magnetic field saturation, we decided to test two initial topologies of the magnetic field shown in the left panels of Fig. 1. The top sub-panel shows the initial quadrupolar configuration for models Q and Q( $2\pi$ ). The bottom sub-panel shows the dipolar topology used to initialize model D. In both cases the magnetic field was normalized not to exceed  $p_{\text{mag}}/p_{\text{gas}} = 1/20$  in the domain. We stress here that little is known about large scale magnetic fields in accretion flows and both configurations must be somewhat arbitrary.

In the global sense both topologies have zero net-flux of magnetic field - the loops are contained in the torus and in the computational domain. However, as accretion proceeds, one may expect that portions of the torus located at different radii will approximately proceed in order towards the BH. According to this picture, the quadrupolar topology would correspond to zero net vertical flux, in contrast to the dipolar topology where the vertical field does not cancel out at given radius.

For both configurations the net radial flux at given radius is zero. However, the two are not identical in this aspect. The quadrupolar topology is asymmetric – the positive radial magnetic field is located near the equatorial plane and the negative field near the torus surface. If only the latter escapes the bulk of the disk, e.g., buoyantly or dragged by outflowing gas, then one may expect non-zero radial net flux left in the disk. Similar effect would take place if the clock- and counter-clockwise loops are not advected in parallel – one of the loops may dominate the inner region but the presence of the other one would make the first asymmetric with respect to the equatorial plane.

## 4 ACCRETION AND ULTIMATE MAGNETIC FIELD

Figure 2 shows the history of the accretion rate through the BH horizon for the simulated models. Simulation Q (blue line) accreted

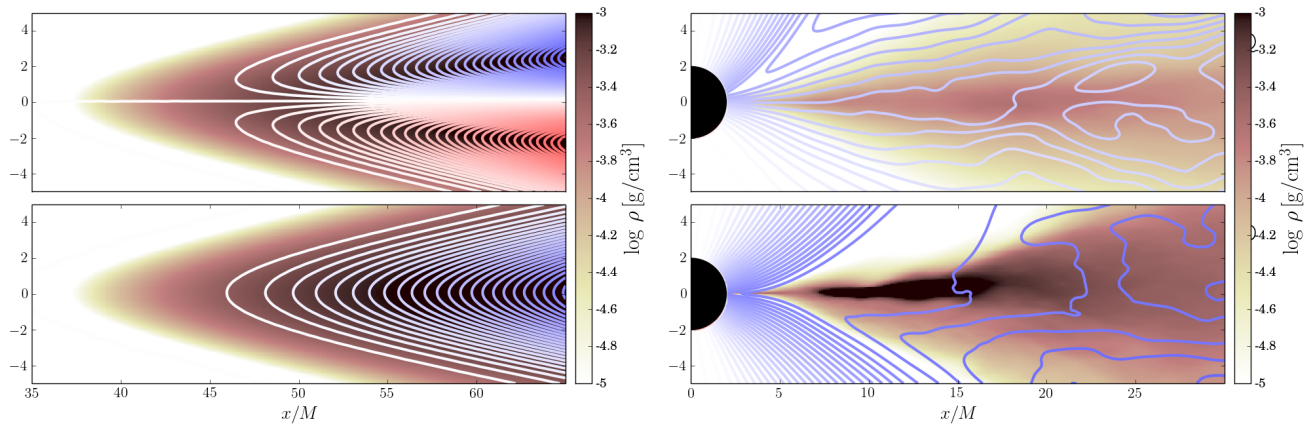


**Figure 1.** Left panels: Initial configuration of density and the magnetic field in simulations Q (top) and D (bottom panel). Colors denote clock- (red) and anti-clockwise (blue) loops. Right panels: Magnetic field averaged over time and azimuth for the same simulations corresponding respectively to  $t = 5000 \div 20000t_g$  and  $t = 2500 \div 7500t_g$ . Simulation Q (top sub-panel) shows much more significant radial net flux of magnetic field which results in stronger magnetization.

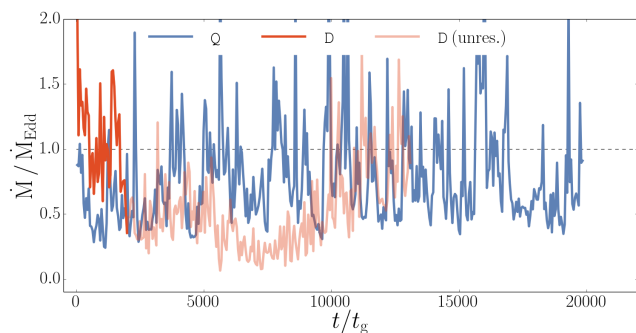


**Figure 2.** The history of accretion rate through the BH horizon for the thin disk simulations. The weakly magnetized simulation D became under-resolved after ca.  $2000t_g$ .

at relatively steady state with average accretion rate of ca.  $0.8\dot{M}_{\text{Edd}}$ . The inflow/outflow equilibrium, i.e., the region where the accretion rate is constant, extended in this case to  $r \approx 15r_g$ . The other simulation, D (red line), did not show a steady state – the accretion rate fell down initially from  $\sim 1\dot{M}_{\text{Edd}}$  to  $\sim 0.2\dot{M}_{\text{Edd}}$  as a result of unbalanced cooling of the disk. The related collapse, discussed below, led to under-resolving the MRI near the equatorial plane. The initial decrease of the accretion rate was followed by an increase and return to the original rate  $\sim \dot{M}_{\text{Edd}}$ . However, the under-resolved equatorial region makes this stage of the simulation unreliable.

Right panels of Fig. 1 show the average configuration of the magnetic field in the saturated state of simulation Q (top) and in the decline phase of simulation D (bottom sub-panel). There is a qualitative difference between the two. The latter, initiated with a dipolar magnetic field, led to magnetic field roughly symmetric with respect to the equatorial plane. Some amount of magnetic flux has accumulated at the BH and the bulk of the disk is threaded by mostly vertical net magnetic field. There is no significant radial component present.

It is not the case for the simulation initiated with the quadrupolar field (Q, top sub-panel). One of the set of loops (the counter-clockwise) preceded the other and dominated the innermost region. However, it did not form a symmetric configuration like in the other case – the positive radial magnetic field covers larger volume and, in particular, dominates in the bulk of the disk. The mag-

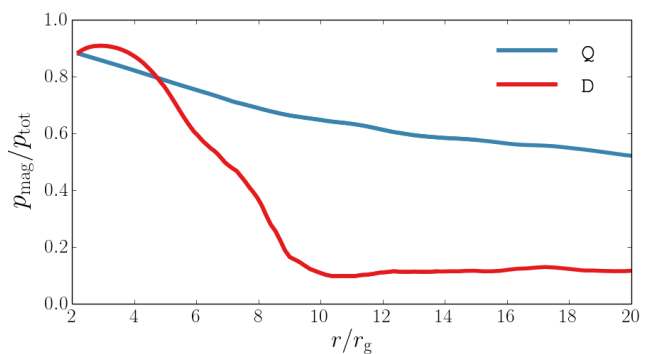


**Figure 3.** The ratio of magnetic to total pressures averaged within the disk density scaleheight for models Q and D corresponding respectively to  $t = 5000 \div 20000t_g$  and  $t = 2500 \div 7500t_g$ . Significant net radial magnetic flux in the disk results in magnetically supported accretion.

netic pressure corresponding to the net radial component amounts to  $\sim 0.0015$  of the total pressure at radius  $\sim 15r_g$ .

As discussed before, non-zero radial magnetic flux in a shearing flow leads to a rapid grow of the azimuthal component and, as a result, of the magnetic pressure. Fig. 3 compares the magnetic pressure contribution to the total pressure between the simulations. Simulation D, which did not develop significant radial flux, shows magnetic pressure contributing to ca. 10% of the total pressure for  $r \gtrsim 10r_g$ , in agreement with the standard MRI saturation state. The other model, however, the one with non-zero net radial flux of magnetic field in the disk, has much different properties – the magnetic pressure grows so much that it dominates the pressure budget. Near the edge of the inflow/outflow equilibrium ( $r \approx 15r_g$ ) the magnetic field provides 60% of the total pressure. The quadrupolar initial configuration of magnetic field led to the magnetically supported disk state (compare Machida et al. 2006).

## 5 HEATING AND COOLING

The qualitative difference in the accretion rate history suggests that only the strongly magnetized disk (model Q) can maintain the sub-Eddington state. In this section we study the balance between heating and cooling in the simulations.

Calculating the two is trivial for the simulations of accretion

disks in a shearing box where the gas is confined to the box and one may study the evolution of the heat content in the same volume of gas for a long time (Jiang, Stone, & Davis 2013). It is no longer straightforward in global simulations such as discussed in this work. The reason is that the gas does not stay in one location but moves in a turbulent way inward.

It may seem that following the same parcel of gas along its way towards the BH is the best approach to calculate heating and cooling in a global simulation and we apply it below (Section 5.2). However, the heating and cooling rates depend on the location, and, for simulations with limited range of inflow/outflow equilibrium, one can follow the gas no longer than its inflow time.

Another approach is to study the gas properties at fixed radius. In this way one may expect fixed heating and cooling rates, but one also has to deal with different parcels of gas crossing a given radius at a given time. Only if the system is in equilibrium, i.e., the average accretion rate and disk properties do not change with time, one may say that at fixed radius one probes different random (turbulent) realizations of the same averaged state. We apply this method below as well (Section 5.1).

To study the heating and cooling rates we define a “box” enclosed by two radial boundaries and the vertical boundary at the polar angle  $\theta = 55^\circ$  (simulation Q) and  $\theta = 65^\circ$  (D), corresponding to the approximate locations of the photosphere in the respective simulations (see the topmost panel of Fig. 8 for the photosphere location in model Q), and covering the full azimuthal extent of a given simulation. The cooling rate is defined as the rate at which radiative flux crosses the vertical boundaries of the box. The heating rate is estimated by calculating the rate at which gas transfers energy to the radiation field, i.e., by integrating the time component of the radiative four-force,  $G_t$  (turbulent dissipation increases internal energy of the gas, but gas immediately releases photons to maintain local thermal equilibrium<sup>2</sup>).

## 5.1 Eulerian picture

We start studying heating and cooling by calculating the respective rates at a fixed location. The radial boundaries of the boxes were set at  $r = 14r_g$  and  $16r_g$  for simulation Q and at  $r = 10r_g$  and  $11r_g$  for simulation D (the choice was motivated by the condition that the boxes are inside the inflow/outflow equilibrium region and far enough from the BH so that the effect of radial advection of heat is negligible).

Figure 4 shows the heating and cooling rates calculated at these locations for model Q (top) and D (bottom panel) as a function of time. For the former, the cooling rate follows the viscous heating rate closely throughout the simulation and on average corresponds to the rate predicted by the standard thin disk model for accretion rate  $0.8\dot{M}_{\text{Edd}}$ . The magnetic contribution to the total pressure stays in this case at the level of 60%. The behavior of the weakly magnetized simulation D (bottom panel) is qualitatively different. From the beginning the cooling rate significantly exceeds the heating rate. As a result, the disk cools down, collapses towards the equatorial plane, and the MRI becomes under-resolved at the equatorial plane for  $t \geq 2000t_g$  (the corresponding  $Q^0$  parameter drops below 10, see Hawley et al. (2013)). Because of cooling dominating over heating, the thermal and radiation pressures keep decreasing, and ultimately (for  $t \geq 8000t_g$ ), the magnetic pressure dominates the total pres-

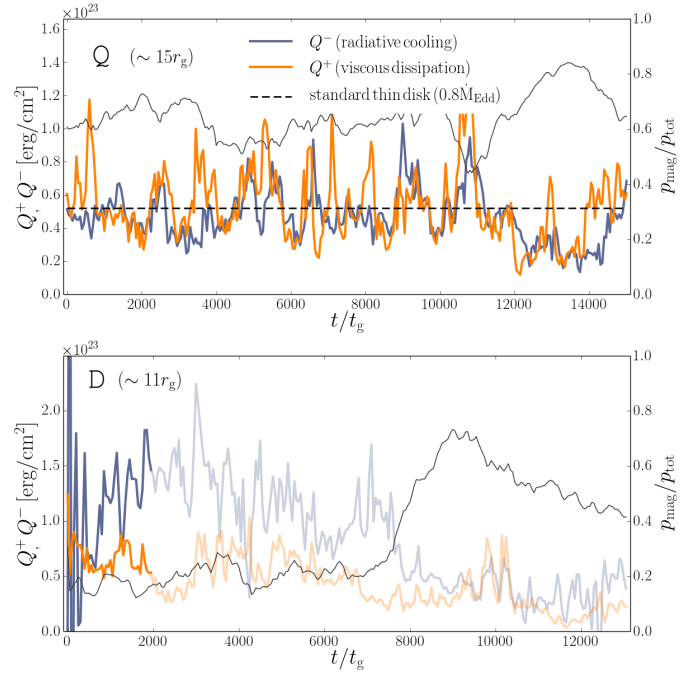


**Figure 4.** Heating ( $Q^+$ , orange lines) and cooling ( $Q^-$ , blue lines) as a function of time calculated at  $r \approx 15r_g$  and  $r \approx 11r_g$  for the stable simulation Q (top) and the unstable simulation D (bottom panel), respectively. The solid black line shows the magnetization parameter  $\beta' = p_{\text{mag}}/p_{\text{tot}}$ . The semi-transparent section of lines in the bottom panel reflect the period when the MRI was under-resolved at the equatorial plane.

sure. Whether such a state can be maintained by itself will have to be verified numerically in a separate, higher resolution, study.

Figure 5 shows the heating/cooling rates as a function of the (averaged over volume) radiation pressure for the stable, strongly magnetized model Q (left panel) and the collapsing model D (right panel). Two sets of markers are plotted. The grey markers show the radiative cooling rates. The other set of markers shows the heating rates and their colors denote the time when they were calculated. For the magnetically supported disk (left panel) the heating and cooling rates virtually overlap each other proving the thermal equilibrium of the disk. There is no clear temporal trend, i.e., the radiation pressure stays close to  $3 - 4 \times 10^{14}$  erg/cm<sup>3</sup> at all times. It is also evident that the rate of radiative cooling is proportional to the radiation pressure, consistent with the diffusive radiation transfer. Similar dependence is shown by the rate of viscous dissipation, in reasonable agreement with Eq. 10, which for  $\beta' = 0.6$  predicts thermally stable slope of  $s = 0.8$ .

The right panel shows the same quantities for simulation D. In this case there is no equilibrium state – the accretion rate changes significantly with time and the gas crossing given box is not expected to show consistent properties. This is indeed the case. As noticed before, the cooling rate exceeds the heating rate as long as the magnetization is low, i.e.,  $\beta' \lesssim 0.5$ . The radiation pressure initially drops down consistently with time showing once again that the disk was out of thermal equilibrium. It stabilizes around  $10^{14}$  erg/cm<sup>3</sup> only in the late ( $t \geq 11000t_g$ ), strongly magnetized, but underresolved stage.

<sup>2</sup> What would not be the case for optically thin disks.

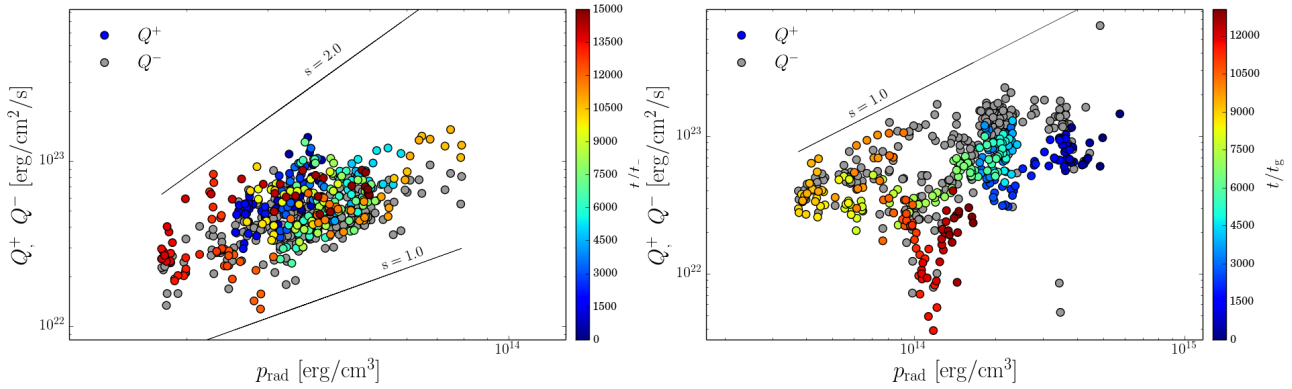


**Figure 5.** Heating ( $Q^+$ , color markers) and cooling ( $Q^-$ , grey markers) rates at  $r \approx 15r_g$  for the stable simulation Q (left panel) and the unstable simulation D (right panel) as a function of the average radiation pressure,  $p_{\text{rad}}$ . The values were extracted near radius  $r = 15r_g$  and  $r = 11r_g$  for models Q and D, respectively. Colors of the markers denote the magnetic to total pressure ratio.

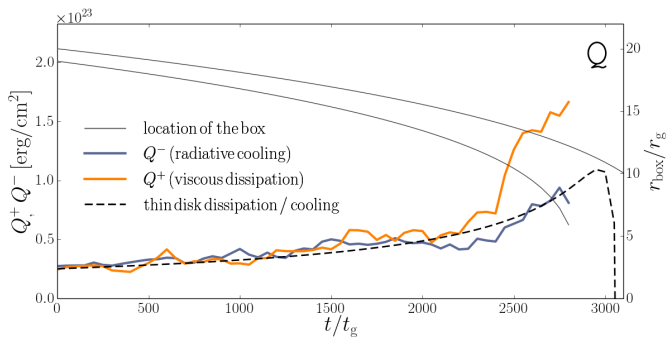


**Figure 6.** Heating (orange) and cooling rates (blue lines) in a box infalling with the average radial velocity of the gas for simulation Q. The radial boundaries of the box were initially located at  $r = 19r_g$  and  $20r_g$ . The thin black lines show their location as a function of time.

## 5.2 Lagrangian picture

We now study the heating/cooling balance by following the gas on its way towards the BH inside the inflow/outflow equilibrium region. Because such an equilibrium has not been reached for simulation D, we limit ourselves here to the stable simulation Q. We first approximate the average radial velocity of the flow between radii  $r = 6r_g$  and  $20r_g$  and get  $v_Q = -3(r/r_g)^{-2.5}$ . Then, we “drop” a box, initially located between  $r = 19r_g$  and  $20r_g$ , and calculate the heating/cooling rates on its way towards the BH.

Figure 6 shows the radiative cooling (blue line) and viscous heating (orange line) rates as a function of time and the corresponding location of the box (denoted with the black line labeled on the right) for the stable simulation Q. The profiles were obtained by averaging the properties of five separate boxes “dropped” at different times. The dashed line shows the emission profile predicted by the thin disk model for  $0.8\dot{M}_{\text{Edd}}$  at the location corresponding to the center of the box.

The simulated disk shows exact balance between heating and cooling in the initial stage of the box infall – this indicates that the disk is radiatively efficient, i.e., all the generated heat is taken away from the disk by radiation. At the same time the disk neither cools nor heats up, but maintains the equilibrium state it has reached. When the inner boundary of the box is located inside  $r \approx 11r_g$  (what happens roughly after  $t = 2200r_g$ ), the rate of viscous heating starts to exceed the rate of radiative cooling (calculated by inte-

grating radiative flux over the vertical boundaries). However, most of the excess heat is ultimately deposited on the BH as a result of both strong collimation of the radiation (which was emitted in gas moving with relativistic velocity towards the BH and crosses the inner radial box boundary, instead of escaping vertically) and photon trapping. The rate of radiative cooling, i.e., the rate at which radiation escapes from the system, follows closely the prediction of the standard model (denoted with the dashed line).

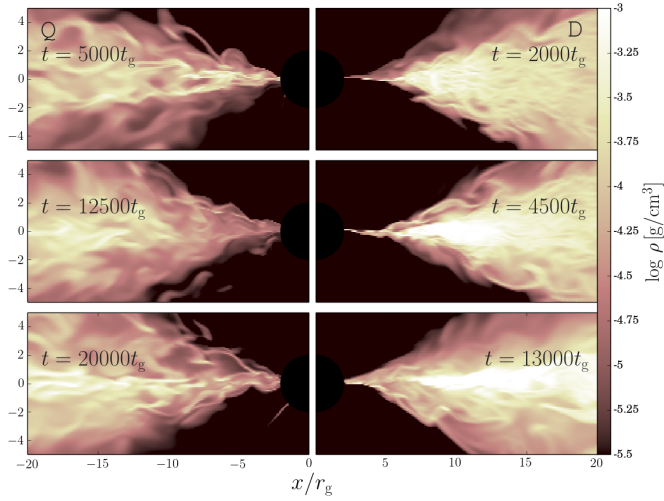
## 6 COLLAPSING, WEAKLY-MAGNETIZED DISK

Figure 7 compares the evolution of the two models over time. The left set of panels shows the magnetically supported disk. It maintains its thickness and properties throughout the simulation. The right panels reflect the evolution of the weakly magnetized disk which changes its properties on a relatively short (thermal) timescale. Because of the excess of cooling over heating, the disk loses its radiation pressure support and gas collapses towards the equatorial plane. The density and the amount of gas in that region increase, and the MRI becomes under-resolved.

Because of the cooling rate initially significantly exceeding the heating rate, the radiative content of the collapsing disk decreases and the magnetic field (dominated by the toroidal component preserved during the collapse) becomes more and more significant (Machida et al. 2006). We indeed observe that the latest stages of the evolution of model Q become magnetic pressure supported (Fig. 4). However, limited resolution of our simulation does not allow us to study this state in detail. It is an open question whether the disk manages to stay in such strongly magnetized (and therefore stable) state, despite the fact that there was hardly any net radial flux of magnetic field before the collapse, or rather the limit-cycle behavior (Lasota & Pelat 1991; Szuszkiewicz & Miller 1998) of the accretion flow leading to strongly varying accretion rate (and luminosity) on timescales of the order of hours ( $1h \approx 10^8 t_g$ ) occurs.

## 7 PROPERTIES OF THE STABLE SOLUTION

Having identified the crucial role of magnetic field in stabilizing disks at sub-Eddington accretion rates, we now look more closely at the properties of the stable solution. We note, however, that the solution we obtained is not unique. We suspect that the exact proper-



**Figure 7.** Time evolution of the strongly (model Q, left panels) and weakly (model D, right panels) magnetized disks. Only the magnetically supported disk retains the equilibrium state. The weakly magnetized one cools down, collapses towards the equatorial plane and leads to under-resolving the MRI.

ties of the disk will depend on the large-scale properties of the magnetic field. Our simulation started with an arbitrary magnetic field setup and evolved into a strongly magnetized state which proves the concept, but does not have to be typical for the magnetically supported mode of accretion. Further numerical work is necessary to get more understanding of such accretion flows.

Figure 8 presents a number of disk properties on the poloidal plane basing on the averaged (left) and snapshot (right halves of the panels) data. The first panel from the top shows the distribution of gas density,  $\rho$  (colors), together with the photosphere location (with respect to the total opacity, solid lines) and the density scaleheight,  $h = \sqrt{\int \rho z^2 dz / \int \rho dz}$  (dashed lines). The gas is clearly turbulent and only moderately concentrated at the equatorial plane. Although the scaleheight is not large ( $h/r \approx 0.15$ ), the photosphere is quite far from the equatorial plane. Such a density distribution results from the fact that the magnetic pressure provides support against vertical gravity and prevents significant compression of gas at the equatorial plane.

The second panel shows the gas temperature,  $T_{\text{gas}}$ . Near the equatorial plane, the gas is roughly at  $10^{7.5} K$  in the whole inner region. Much higher temperatures are near the axis where the density is the lowest, and magnetization is the largest. The distribution of temperature shows a slight assymetry caused by the assymetric distribution of net magnetic field (compare Fig. 1).

The third panel shows the energy density in the radiation field measured in the comoving frame of gas,  $\bar{E}$  – a quantity that in optically thick gas reflects distribution of the radiation pressure

The fourth panel shows the magnetic to total pressure ratio,  $\beta'$ . The whole inner region is dominated by the magnetic pressure. Even at the equatorial plane, where the radiation pressure is largest, magnetic pressure dominates the pressure balance. Near the scaleheight, but still below the photosphere, the magnetic pressure contributes to 70-80% of the total pressure. Once again, the assymetry in the polar region is visible.

The fifth panel shows the radiation to gas pressure ratio,  $\beta_{\text{rad}}$ . The radiation pressure itself overwhelms the thermal pressure of gas by roughly three orders of magnitude in the whole domain.

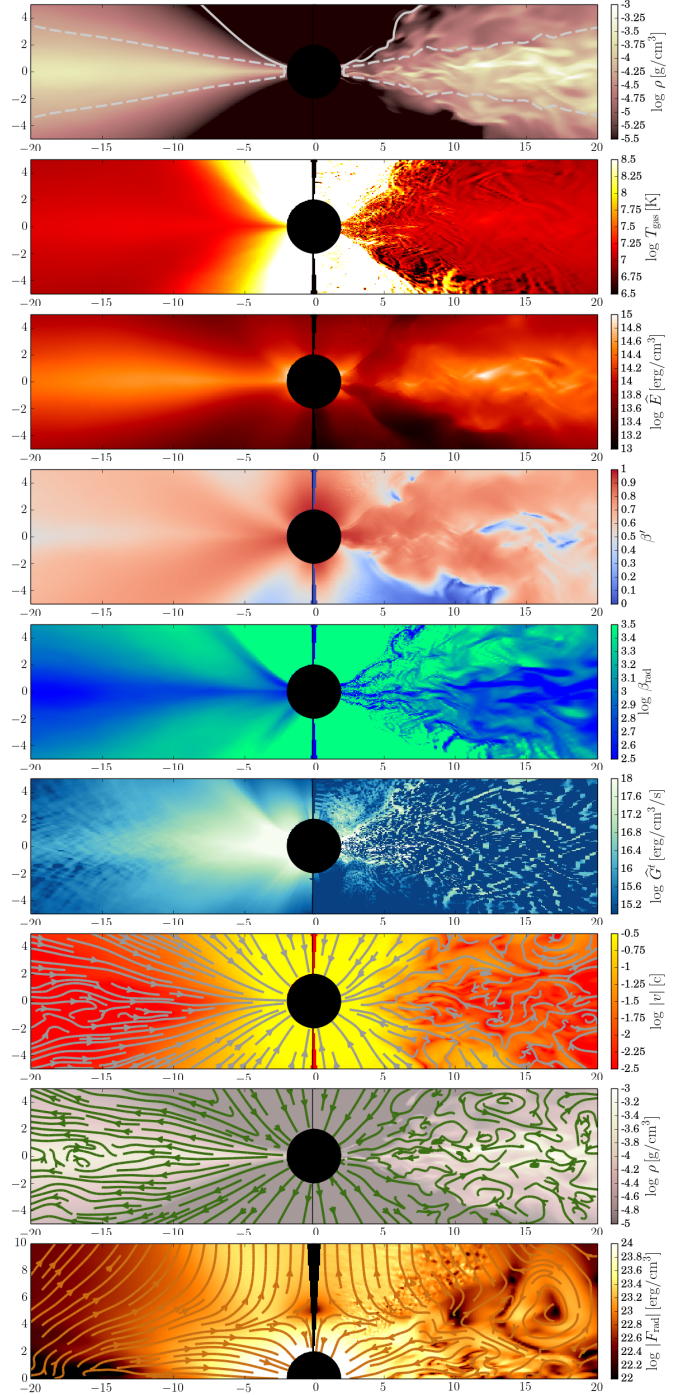


**Figure 8.** Comparison of time and azimuth averaged (left panels) and snapshot data (right panels) from the stable model Q reflecting, from top to bottom, gas density,  $\rho$ , gas temperature,  $T_{\text{gas}}$ , comoving radiative energy density,  $\bar{E}$ , magnetic to total pressure ratio,  $\beta'$ , radiation to gas pressure ratio,  $\beta_{\text{rad}}$ , heating rate,  $\bar{G}$ , magnitude and direction of gas velocity,  $v$ , poloidal magnetic field,  $B^p$  (plotted on top of gas density), and magnitude and direction fo radiative flux,  $F_{\text{rad}}$ . The solid and dashed lines in the topmost panel show the locations of the photosphere and density scale-height, respectively.

The sixth panel shows the viscous heating rate, equal to the photon generation rate,  $\widehat{G}$ . On average, it is positive and reflects energy transfer from heated gas to the radiation field. The dissipation takes place throughout the disk volume, and not only at the equatorial plane, with significant amount of energy released just below the photosphere and close to the BH horizon.

The seventh panel reflects the velocity field of the disk. On average, the gas approaches the BH at all polar angles, even in the polar region (what would presumably change if the BH was rotating and could produce, even moderate, jet). The gas moves on average with the lowest velocity near the equatorial plane. The surface layers fall on the BH with noticeably larger velocity. As a result, the accretion is not limited to the most dense equatorial region, but the surface layers bring inward comparable amount of gas.

The eighth panel (second from the bottom) shows the average and temporal magnetic field. The average properties have already been discussed in context of Fig. 1. The magnetic field is not symmetric with respect to the equatorial plane – magnetic pressure is higher in the upper polar funnel and the net radial flux in most of the disk is positive, causing significant growth of the magnetic field and ultimately leading to the magnetically supported state.

The bottommost panel in Fig. 8 shows the properties of the radiation field. Colors denote the magnitude of the local radiation flux and vectors show its direction. For  $r \gtrsim 10r_g$  the radiation diffuses out of the disk in the direction roughly perpendicular to the photosphere. Inside that radius, there is significant component of radiation flux pointing towards the BH – these are the photons which are either trapped in the optically thick gas or were emitted, and therefore collimated, by gas rushing towards the horizon. The radiation flux has the largest magnitude inside the innermost stable orbit (ISCO) due to the strong dissipation there (compare the sixth panel), but all that radiation ends up ultimately under the horizon.

## 8 LUMINOSITY AND ENERGY FLOWS IN THE STABLE SOLUTION

We now briefly discuss energy flow in the magnetically supported, sub-Eddington disk, basing on previously discussed in detail model Q. We will follow closely the approach developed in Sądowski et al. (2016). The total flux of energy is decomposed into the binding, radiative and viscous fluxes. Binding energy is transported with the gas which approaches the BH on roughly Keplerian orbits and liberates its own binding energy (the sum of gravitational and kinetic energies). Radiative energy is transported either outward by free streaming photons escaping the system, or inward by photons trapped in optically thick gas or collimated towards the BH. Viscous energy transport results from the effective viscosity transferring rotational energy between adjacent disk annuli. In a steady state, the three sum up to the total, independent of radius, energy extracted from the system. In the standard thin disk model, this total energy (or luminosity) equals to the (minus) binding energy of the gas crossing the horizon and, at the same time, to the radiative luminosity of the system as seen from infinity, i.e., to  $5.7\% \dot{M}c^2$  for a non-rotating BH (5.7% is the radiative efficiency of the system).

Figure 9 shows such a decomposition of the total energy flux for simulation Q based on time and azimuth averaged data. The total energy, denoted by the thick solid red line, is constant to 10% within  $r \approx 20r_g$  (the departure from a constant value suggests that the properties of the disk change a bit with time). The total luminosity of the system is very close to the thin disk luminosity (denoted by the red dashed line), and equals  $5.5 \pm 0.5\% \dot{M}c^2$ .

The binding energy (blue solid line) is also close to the thin disk counterpart (blue dashed line) outside the innermost stable orbit ( $r_{\text{ISCO}} = 6r_g$ ). This fact reflects almost Keplerian angular momentum of the gas in the discussed simulation and relatively insignificant radial velocity contribution. The behavior is, however, qualitatively different inside the ISCO. While in the standard thin disk model there is no torque acting on the gas inside that radius (Paczynski 2000)<sup>3</sup> and binding energy is constant in the plunging region, the numerical solution shows that gas becomes more and more bound after crossing ISCO and, as a result, more and more energy is transported as binding energy. This means that significant stresses act inside ISCO, what should not be surprising having in mind how strongly magnetized the gas is (see Noble et al. (2010), but also Shafee et al. (2008); Penna et al. (2010); Kulkarni et al. (2011)).

The profile of radiative luminosity is also very close to the thin disk profile (compare solid and dashed orange lines). At radius  $r = 15r_g$  radiative flux carries out  $\sim 1\% \dot{M}c^2$ , only ca. 10% less than the standard model predicts. The behavior in the innermost region is, however, again very different. According to the standard thin disk model, no radiation crosses the ISCO or is generated inside that radius. In this numerical simulation, on the contrary, significant dissipation takes place in the innermost region. Nevertheless, most of the radiation emitted there ends up inside the BH because it is either trapped in the flow or is strongly collimated towards the BH (compare the bottommost panel of Fig. 8). Photons crossing the horizon carry roughly  $2\% \dot{M}c^2$ .

Finally, the viscous flux of energy once again agrees well in the outer region with the predictions of the analytical thin disk modeling but disagrees in the innermost ( $r \lesssim 10r_g$ ) region where noticeable viscous energy transport takes place, in disagreement with the standard modeling.

To sum up, the simulated magnetically supported thin disk shows significant dissipation and stress inside the ISCO, in the so-called plunging region, inconsistent with the standard model. However, somewhat surprisingly, the energetics of the disk far from the BH agrees very well with the standard modeling. The extra energy extracted in the innermost region does not have a chance of being observed from infinity<sup>4</sup>. Whether this is true also for thinner, less optically thick disks, corresponding to lower accretion rates, has to be verified numerically in the future.

## 9 DISCUSSION

### 9.1 Net flux of magnetic field

We have shown that thin and radiatively efficient accretion disks are thermally stable when dominated by magnetic pressure. The necessary condition for the stability is strong magnetic support which is provided mainly by the azimuthal component of the field. In the case of our stable simulation (model Q) such strong azimuthal field developed as a result of non-zero radial flux of magnetic field inside the disk. Are astrophysical accretion disks likely to have significant net radial flux?

<sup>3</sup> Paczynski (2000) has shown that the torque at the inner edge disappears if only angular momentum is conserved, disk is thin ( $h/r \ll 1$ ), and the viscosity parameter is small ( $\alpha \ll 1$ ). In our solution the last condition is not satisfied, with  $\alpha \approx 0.3$  at ISCO and reaching 0.9 near  $r = 3r_g$ .

<sup>4</sup> Similar conclusion was reached by Zhu et al. (2012) who studied radiation from artificially cooled thin MHD disks.



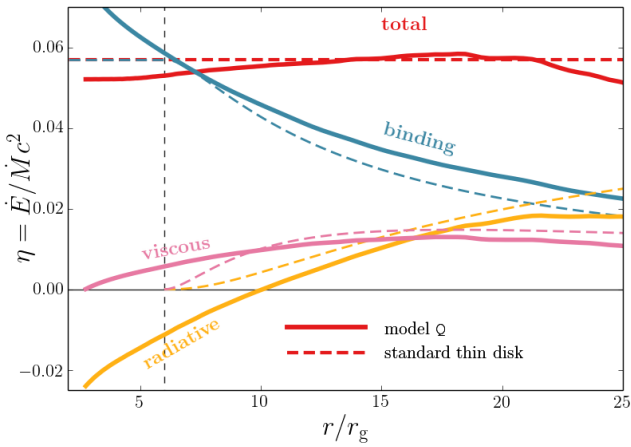


**Figure 9.** Energy flow through the stable simulation Q (solid lines) compared to the thin-disk solution (dashed lines).

It is tempting to expect that the origin of such a large-scale field is the advection of the field by the gas in the accretion disk from the interstellar medium or a companion star. If only such a field is not perfectly dipolar (or uneven-polar) one may expect that the asymmetry leads to effectively a non-zero radial flux in the bulk of the disk. However, whether or not the large-scale field can be advected into the innermost region depends on the balance between the advection and diffusion of the field. Standard geometrically thin disks are unlikely to drag significant amount of magnetic field on to the BH (Lubow et al. 1994; Ghosh & Abramowicz 1997). However, as Guilet & Ogilvie (2012, 2013) found, if one takes into account the vertical structure of the disk, the advection of magnetic flux can be much faster than found originally. Indeed, it may be the case for the strongly magnetized solutions discussed here which not only show much larger radial velocities than the standard model predicts, but also the velocities increase significantly towards the surface of the disk.

There is also another way of obtaining an accretion disk dominated by magnetic pressure which, on the contrary, does not require (at least initially) efficient advection of magnetic field. As Machida et al. (2006) pointed out, when an X-ray binary undergoes the transition from the low/hard state (corresponding to low accretion rates and low optical depths) to the high/soft state (at larger accretion rates), the disk starts to cool and shrinks in the vertical direction while almost conserving the toroidal magnetic flux (we see such behavior in the collapse of model D). Such a process leads to a cooler, magnetically supported, quasi-steady state. Machida et al. (2006) have shown that such a configuration can exist for at least the thermal time. Whether it can survive for much longer times, without relaxing to the lower magnetization state implied by local, zero-flux numerical studies, has still to be verified (note recent work by Wielgus et al. 2015).

## 9.2 Observables

The magnetically supported thin disks, an example of which has been presented in this work, differ from the standard model of thin disks (Shakura & Sunyaev 1973) in two aspects. Firstly, they are supported by magnetic pressure, not the radiation pressure, although the two have similar magnitudes. This fact results in a disk thicker than standard one at the same radius and accretion rate. The

effective color temperature is also higher because the photosphere is now located in the strongly magnetized, hot region where photons are efficiently up-scattered by hot electrons. Secondly, the high magnetization implies significant stresses taking place at and inside ISCO. As a result, radiation is efficiently generated in the plunging region, in contrary to the assumptions of the standard model. However, for the slightly sub-Eddington disk presented in this work, all this excess of generated radiation is advected on the BH, and the luminosity of the system, as seen from the distance, very well agrees with the efficiency of the standard disks.

What would such a magnetized thin disk system look like? Because the extra radiation generated by dissipation in the plunging region does not escape, one may expect similar luminosities to the predicted by the standard model. However, the spectrum may look different. Thicker disk would imply larger color temperature and harder spectrum (what would bring continuum-based BH spin estimates down). Also a stronger inclination dependence may be expected. Better answers will be provided once detailed frequency- and angle-resolved calculations of the radiation transfer based on numerical simulations like ours are performed.

## 10 SUMMARY

We have performed two three-dimensional, global, general relativistic, radiative simulations of sub-Eddington accretion disks. The simulations were initialized with different configurations of the magnetic field. One of them evolved into a magnetically supported state in thermal equilibrium with strong magnetic field maintained by a non-zero radial magnetic flux in the bulk of the disk. The other did not develop strong magnetic field, showed consisted excess of cooling over heating and continued collapsing towards the equatorial plane. We summarize our conclusions as following:

(i) *Thermal stability:* – We have shown that magnetic pressure dominated thin, sub-Eddington accretion disks can maintain thermal equilibrium, in contrast to thermally unstable disks dominated by radiation pressure.

(ii) *Magnetization:* – The strong magnetization required for stabilization of thin disks results either from the presence of a non-zero radial magnetic flux (what requires efficient advection of large-scale magnetic field by the disk), or from the collapse of previously thick disk during the hard to soft transition.

(iii) *Standard model:* – The magnetically supported thin disks are thicker than standard ones at the same radius and accretion rate. They also show significant dissipation inside ISCO. Radiation released in this region, however, does not escape but is advected on the BH. Whether this statement is true for lower accretion rates than simulated here ( $0.8M_{\text{Edd}}$ ) has still to be verified.

(iv) *Luminosity:* – Despite strong dissipation and torque inside ISCO, the efficiency of the simulated disk ( $5.5 \pm 0.5\%$ ) turns out to be very close to the prediction of the standard model (5.7%). The spectrum of the observed radiation, however, is likely to be harder due to the photosphere extending further away from the equatorial plane. Detailed spectral calculations of this mode of accretion will follow.

## 11 ACKNOWLEDGEMENTS

The author thanks David Abarca for his contribution and Ramesh Narayan, Jean-Pierre Lasota and Marek Abramowicz for helpful comments. The author acknowledges support for this work by

NASA through Einstein Postdoctoral Fellowship number PF4-150126 awarded by the Chandra X-ray Center, which is operated by the Smithsonian Astrophysical Observatory for NASA under contract NAS8-0306. These authors O. The author acknowledges computational support from NSF via XSEDE resources (grants TG-AST080026N and TG-AST150019), and from NASA via the High-End Computing (HEC) Program through the NASA Advanced Supercomputing (NAS) Division at Ames Research Center. The author was supported in part by NSF grant AST1312651 and NASA grant TCAN NNX14AB47G. The author also acknowledges support from the International Space Science Institute.

## REFERENCES

- Abramowicz, M. A., Czerny, B., Lasota, J. P., & Szuszkiewicz, E. 1988, *Astrophysical Journal*, 332, 646
- Balbus, S. A., & Hawley, J. F. 1991, *Astrophysical Journal*, 376, 214
- Bai, X.-N., & Stone, J. M. 2013, *Astrophysical Journal*, 767, 30
- Begelman, M. C., & Pringle, J. E. 2007, *Monthly Notices of the Royal Astronomical Society*, 375, 1070
- Begelman, M. C., & Armitage, P. J. 2014, *Astrophysical Journal Letters*, 782, L18
- Ciesielski, A., Wielgus, M., Kluźniak, W., et al. 2012, *Astronomy & Astrophysics*, 538, A148
- Coriat, M., Fender, R. P., & Dubus, G. 2012, *Monthly Notices of the Royal Astronomical Society*, 424, 1991
- Davis, S. W., Stone, J. M., & Pessah, M. E. 2010, *Astrophysical Journal*, 713, 52
- Ghosh, P., & Abramowicz, M. A. 1997, *Monthly Notices of the Royal Astronomical Society*, 292, 887
- Guilet, J., & Ogilvie, G. I. 2012, *Monthly Notices of the Royal Astronomical Society*, 424, 2097
- Guilet, J., & Ogilvie, G. I. 2013, *Monthly Notices of the Royal Astronomical Society*, 430, 822
- Hawley, J. F., Richers, S. A., Guan, X., & Krolik, J. H. 2013, *Astrophysical Journal*, 772, 102
- Hirose, S., Krolik, J. H., & Blaes, O. 2009, *Astrophysical Journal*, 691, 16
- Janiuk, A., & Misra, R. 2012, *Astronomy & Astrophysics*, 540, A114
- Jiang, Y.-F., Stone, J. M., & Davis, S. W. 2013, *Astrophysical Journal*, 778, 65
- Jiang, Y.-F., Stone, J. M., & Davis, S. W. 2014, *Astrophysical Journal*, 796, 106
- Kulkarni, A. K., Penna, R. F., Shcherbakov, R. V., et al. 2011, *Monthly Notices of the Royal Astronomical Society*, 414, 1183
- Lasota, J. P., & Pelat, D. 1991, *Astronomy & Astrophysics*, 249, 574
- Lasota, J.-P. 2001, *New Astronomy Review*, 45, 449
- Levermore, C. D. 1984, *Journal of Quantitative Spectroscopy and Radiative Transfer*, 31, 149
- Li, S.-L., & Begelman, M. C. 2014, *Astrophysical Journal*, 786, 6
- Lightman, A. P., & Eardley, D. M. 1974, *Astrophysical Journal Letters*, 187, L1
- Lubow, S. H., Papaloizou, J. C. B., & Pringle, J. E. 1994, *Monthly Notices of the Royal Astronomical Society*, 267, 235
- Maccarone, T. J. 2003, *Astronomy & Astrophysics*, 409, 697
- Machida, M., Nakamura, K. E., & Matsumoto, R. 2006, *Publications of the Astronomical Society of Japan*, 58, 193
- McClintock, J. E., & Remillard, R. A. 2006, *Compact stellar X-ray sources*, 39, 157
- McKinney, J. C., Tchekhovskoy, A., Sądowski, A., & Narayan, R. 2014, *Monthly Notices of the Royal Astronomical Society*, 441, 3177
- Noble, S. C., Krolik, J. H., & Hawley, J. F. 2010, *Astrophysical Journal*, 711, 959
- Oda, H., Machida, M., Nakamura, K. E., & Matsumoto, R. 2009, *Astrophysical Journal*, 697, 16
- Ohsuga, K., & Mineshige, S. 2011, *Astrophysical Journal*, 736, 2
- Paczyński, B. 2000, arXiv:astro-ph/0004129
- Penna, R. F., McKinney, J. C., Narayan, R., et al. 2010, *Monthly Notices of the Royal Astronomical Society*, 408, 752
- Penna, R. F., Sądowski, A., Kulkarni, A. K., & Narayan, R. 2013, *Monthly Notices of the Royal Astronomical Society*, 428, 2255
- Pessah, M. E., & Psaltis, D. 2005, *Astrophysical Journal*, 628, 879
- Piran, T. 1978, *Astrophysical Journal*, 221, 652
- Pringle, J. E. 1976, *Monthly Notices of the Royal Astronomical Society*, 177, 65
- Sądowski, A., Narayan, R., Tchekhovskoy, A., & Zhu, Y. 2013a, *Monthly Notices of the Royal Astronomical Society*, 429, 3533
- Sądowski, A., Narayan, R., McKinney, J. C., & Tchekhovskoy, A. 2014b, *Monthly Notices of the Royal Astronomical Society*, 439, 503
- Sądowski, A., Narayan, R., Tchekhovskoy, A., Abarca, D., Zhu, Y., & McKinney J. C. 2014b, in press
- Sądowski, A., Lasota, J.-P., Abramowicz, M. A., & Narayan, R. 2016, *Monthly Notices of the Royal Astronomical Society*, 456, 3915
- Shakura, N. I., & Sunyaev, R. A. 1973, *A&A*, 24, 337
- Shakura, N. I., & Sunyaev, R. A. 1976, *Monthly Notices of the Royal Astronomical Society*, 175, 613
- Shafee, R., McKinney, J. C., Narayan, R., et al. 2008, *Astrophysical Journal Letters*, 687, L25
- Shi, J., Krolik, J. H., & Hirose, S. 2010, *Astrophysical Journal*, 708, 1716
- Szuszkiewicz, E., & Miller, J. C. 1998, *Monthly Notices of the Royal Astronomical Society*, 298, 888
- Wielgus, M., Fragile, P. C., Wang, Z., & Wilson, J. 2015, *Monthly Notices of the Royal Astronomical Society*, 447, 3593
- Zhu, Y., Davis, S. W., Narayan, R., et al. 2012, *Monthly Notices of the Royal Astronomical Society*, 424, 2504